Optical resonances created by photonic transitions

Zongfu Yu[a)] and Shanhui Fan
E. L. Ginzton Laboratory, Stanford University, Stanford, California 94305, USA

(Received 21 June 2009; accepted 5 December 2009; published online 7 January 2010)

We show that a high-Q optical resonance can be created dynamically, by inducing a photonic transition between a localized state and a one-dimensional continuum through refractive index modulation. In this mechanism, both the frequency and the external linewidth of a single resonance are specified by the dynamics, allowing complete control of the resonance properties. An example using photonic crystal heterostructure cavity is demonstrated with numerical simulation. We also show that the reported effect can be accomplished with realistic index modulation strength and frequencies. © *2010 American Institute of Physics*. [doi:10.1063/1.3279130]

Resonance appears when a localized state couples to a continuum. In photonics, of particular interest is when the localized state is supported by an optical microcavity, and the continuum is one-dimensional such as in a waveguide. Such waveguide-cavity configurations find applications in filters, sensors, switches, slow-light structures, and quantum information processing devices.[1–4]

In all applications of resonance, it is essential to accurately control its spectral properties. For the waveguide-cavity resonances, some of the important spectral properties are the resonance frequency, and the *external linewidth* due to waveguide-cavity coupling. The inverse of such linewidth defines the corresponding quality factor (Q) of the cavity.

In this letter, we show that a single high-Q resonance can be created by dynamically inducing a photonic transition between a localized state and a one-dimensional continuum. Since the coupling between the continuum and the localized state occurs *solely* through dynamic modulations, both the frequency and the external linewidth of a single resonance are specified by the dynamics, allowing complete control of its spectral properties.

We start by first briefly reviewing the Anderson–Fano model,[5,6] which describes the standard waveguide-cavity systems

$$H = \omega_c c^+ c + \int \omega_k a_k^+ a_k dk + V \int (c^+ a_k + a_k^+ c) dk. \qquad (1)$$

Here, ω_c is the frequency of a localized state that is embedded inside a one-dimensional continuum of states [Fig. 1(a)] defined by ω_k. $c^+(c)$ and $a_k^+(a_k)$ are the bosonic creation (annihilation) operators for localized and continuum states, respectively. V describes the interaction between them. Such a model supports a resonance at $\omega_0 = \omega_c$, with an external linewidth $\gamma = 2\pi(V^2/v_g)$ (Defined as the full width at half maximum of the resonance peak). Here $v_g \equiv \frac{d\omega_k}{dk}|_{\omega_0}$.

In contrast to the standard Fano–Anderson model, our mechanism is described by the Hamiltonian [Fig. 1(b)]

$$H = \omega_c c^+ c + \int \omega_k a_k^+ a_k dk + (V + V_D \cos(\Omega t)) \int (c^+ a_k + a_k^+ c) dk. \qquad (2)$$

Here, unlike in Eq. (1), we assume that $\omega_k > \omega_c$ for any k. Consequently, the static coupling term $V\int(c^+ a_k + a_k^+ c)dk$ no longer contributes to the decay of the resonance. Instead it only results in a renormalization of ω_c. The localized state decays solely through the dynamic term $V_D \cos(\Omega t)\int(c^+ a_k + a_k^+ c)dk$, which arises from modulating the system. Such modulation induces a photonic transition[7] between the localized state and the continuum. (Experimentally, photonic transition has been recently observed in silicon micro ring resonator structure.[8])

For the Hamiltonian of Eq. (2), one can derive an input-output formalism[9] in the Heisenberg picture, relating $C(t) = c(t)e^{-i\Omega t}$ to the input field operator $a_{\mathrm{IN}}(t)$ as

$$\frac{d}{dt}C = -i(\omega_c + \Omega)C - \frac{\gamma}{2}C + i\sqrt{\gamma}a_{\mathrm{IN}}, \qquad (3)$$

where $\gamma = 2\pi[(V_D/2)^2/v_g]$ with $v_g = \frac{d\omega_k}{dk}|_{\omega=\omega_c+\Omega}$. For an incident wave a_{IN} in the waveguide, the modulated system therefore creates a single resonance at the frequency $\omega_0 = \omega_c + \Omega$. Importantly, unlike the static system in Eq. (1), here both the frequency ω_0 and the external linewidth γ of the resonance are controlled by the dynamic modulation.

We now realize the Hamiltonian in Eq. (2) in a photonic crystal heterostructure[10] [Fig. 2(a)]. The structure consists of a well and two barrier regions, defined in a line-defect waveguide in a semiconductor ($\varepsilon = 12.25$) two-dimensional photonic crystal. In the barrier regions, the crystal has a triangular lattice of air holes with a radius $r = 0.3a$, where a is the lattice constant. The waveguide supports two $TE(H_z, E_x, E_y)$ modes with even and odd modal symmetry [Fig. 2(c), light gray lines]. In the well region, the hole spacing a' along the waveguide is increased to $1.1a$, which shifts the frequencies of the

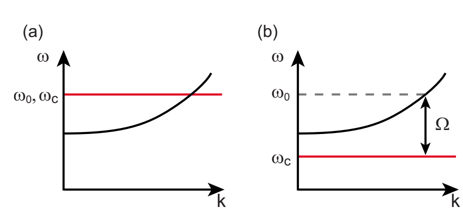

FIG. 1. (Color online) Two different coupling mechanisms between a localized state and a one-dimensional continuum. (a) Static case: The frequency ω_c of the localized state lies in the band of the continuum creating a resonance at $\omega_0 = \omega_c$. (b) Dynamic case: The localized state has its frequency ω_c that falls outside the continuum. A modulation at a frequency Ω creates a resonance at $\omega_0 = \omega_c + \Omega$.

[a)]Electronic mail: zfyu@stanford.edu.

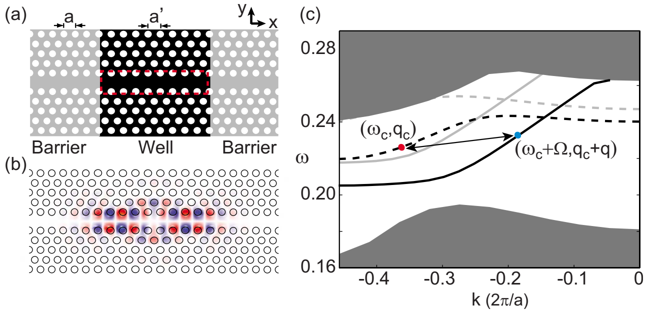

FIG. 2. (Color online) (a) A photonic crystal heterostructure. The width of the waveguide measured from the centers of the holes on the two sides is $1.33a$. The highlighted rectangle represents the modulated region, which has dimensions of $2a\times 9.7a$. (b) Electric field (E_y) profile of a localized state in the well. Red and blue represent positive and negative maximum amplitudes. (c) Dispersion relation of the photonic crystal waveguide modes. The dark and light gray lines are for modes in the well and barriers, respectively. Solid (dashed) lines represent modes with even (odd) modal symmetry. Shadowed regions are the extended modes of the crystal region of the well.

modes downward [Fig. 2(c), dark lines] compared to those of the barriers. As a result, the odd modes in the well and the barriers do not overlap in frequencies. Thus, the well can support localized states, which are essentially standing waves formed by two counter-propagating odd modes in the well. Figure 2(b) shows one such localized state at the frequency $\omega_c=0.2252(2\pi c/a)$, with its corresponding waveguide mode at the wavevector $q_c=-0.37(2\pi/a)$ indicated by a red dot in Fig. 2(c). Without modulation such a localized state cannot leak into the barrier, and hence cannot be excited by wave coming from the barrier.

To induce a photonic transition, we modulate the dielectric constant of the well in the form of $\varepsilon_D=\Delta\varepsilon(y)\cos(\Omega t-qx)$. Here the modulation frequency Ω is chosen such that an even mode in the well at the frequency $\omega_c+\Omega$ can leak into the barriers. The modulation wavevector q is selected to ensure a phase-matched transition between this even mode and the odd mode at (ω_c,q_c) that forms the localized state. Since these two modes have different symmetry, the modulation has an odd transverse profile: $\Delta\varepsilon(y)=\mathrm{sign}(y)\Delta\varepsilon$, with $y=0$ located at the waveguide center.

In the presence of the modulation, we consider an even mode incident from the left barrier, with a frequency ω in the vicinity of $\omega_c+\Omega$. As it turns out, for the even modes, the transmission coefficients into and out of the well are near unity. Thus, inside the well, the amplitudes of the even mode (Fig. 3, blue arrow) at the two edges, $A_{x=0}$ and $A_{x=L}$, are the input and output amplitudes of the system. As the even mode propagates forward from $x=0$ to $x=L$, the modulation induces a transition to a copropagating odd mode at $\omega-\Omega$ (Fig. 3, red arrow). This transition process is described by[11]

$$\begin{pmatrix} A_{x=L} \\ B_{x=L} \end{pmatrix} = \begin{bmatrix} \exp(iLq_{\omega}) & 0 \\ 0 & \exp(iLq_{\omega-\Omega}) \end{bmatrix} \times \begin{pmatrix} \sqrt{1-\eta^2} & i\eta \\ i\eta & \sqrt{1-\eta^2} \end{pmatrix} \begin{pmatrix} A_{x=0} \\ B_{x=0} \end{pmatrix}, \tag{4}$$

where $B_{x=0}$ and $B_{x=L}$ are the amplitudes of the copropagating odd mode at $\omega-\Omega$ at the two edges, q_ω and $q_{\omega-\Omega}$ are the wavevectors of the two modes. For weak modulation, the transition rate $\eta=(\Delta\varepsilon/\varepsilon)L\kappa\ll 1$, where κ is the overlap factor between the two modes and the modulation profile.[11]

Once the fields reach $x=L$, the odd mode is completely reflected, and propagates back to $x=0$. We note that no significant photon transition occurs in the backward propagation, since the modulation profile does not phase-match between $(\omega,-q_\omega)$ and $(\omega-\Omega,-q_{\omega-\Omega})$. Consequently

$$B_{x=0}=\exp(iLq_{\omega-\Omega}+i2\phi)B_{x=L}, \tag{5}$$

where ϕ is the reflection phase at the well edge. Also, since there is a localized state at ω_c, the round trip phase at ω_c is $2(Lq_{\omega_c}+\phi)=2\pi n$ where n is an integer. Therefore, the round trip phase for the odd mode at $\omega-\Omega\approx\omega_c$ can be approximated as

$$2(Lq_{\omega-\Omega}+\phi)\approx 2\pi n+(\omega-\Omega-\omega_c)\frac{2L}{v_{gc}}, \tag{6}$$

where $v_{gc}=\frac{d\omega}{dk}\big|_{\omega=\omega_c}$. Combined Eqs. (4)–(6), the transmission spectrum is

$$T=\frac{A_{x=L}}{e^{iLq_\omega}A_{x=0}}=\frac{\sqrt{1-\eta^2}-e^{i(\omega-\omega_0)2L/v_{gc}}}{1-e^{i(\omega-\omega_0)2L/v_{gc}}\sqrt{1-\eta^2}}\approx\frac{\omega-\omega_0-i\dfrac{\gamma}{2}}{\omega-\omega_0+i\dfrac{\gamma}{2}}, \tag{7}$$

where $\gamma=(\Delta\varepsilon/\varepsilon)^2\kappa^2 Lv_{gc}/2$.

The detailed microscopic theory thus predicts all-pass filter response for this dynamic system consisting of a waveguide coupled to a standing-wave localized state. In contrast, in the static system, coupling of a waveguide to a standing-wave localized state always produces either band-pass or band-reflection filters.[2] Moreover, the resonant frequency

$$\omega_0=\omega_c+\Omega, \tag{8}$$

and the quality factor

$$Q_e\equiv\frac{\omega_0}{\gamma}=\left(\frac{\varepsilon}{\Delta\varepsilon}\right)^2\frac{2\omega_0}{\kappa^2 Lv_{gc}}, \tag{9}$$

are completely controlled by the modulation, in agreement with the phenomenological model [Eq. (3)].

We numerically test the theory using finite-difference time-domain simulations.[12] We simulate a well with a length of $9.9a$. Such a well supports the localized state shown in Fig. 2(b). The length of the modulated region $L=9.7a$ [Fig. 2(a)]. We excite the even modes in the left barrier, with a Gaussian pulse centered at $0.235(2\pi c/a)$, and a width of $0.001(2\pi c/a)$. Without the modulation, the transmission coefficient [Fig. 4(a)] is near unity. With the modulation, (with a strength $\Delta\varepsilon/\varepsilon=1.63\times 10^{-2}$, a frequency $\Omega=9.8$

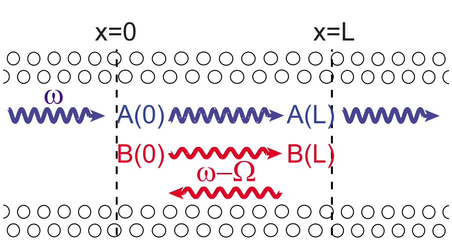

FIG. 3. (Color online) The microscopic theory for photonic transition in the photonic crystal heterostructure. Incident light from the barrier at a frequency ω, as represented by the blue arrows, couples to a mode of the well at the frequency $\omega-\Omega$, as represented by the red arrows. The dashed lines indicate the edges of the well.

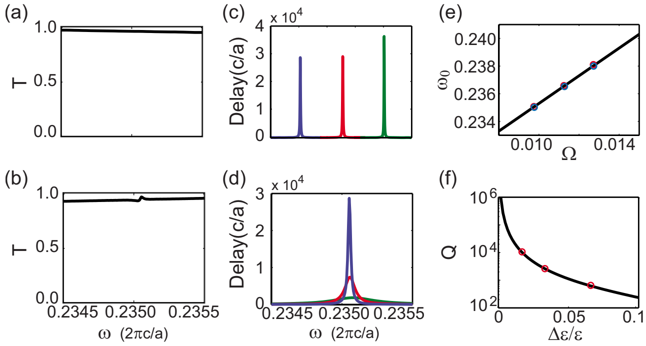

FIG. 4. (Color online) Theory and simulation for the photonic transition process for the structure in Fig. 2. (a) Transmission spectrum for the unmodulated structure. (b) Transmission spectrum in the presence of modulation. The modulation has a frequency $\Omega=9.8\times10^{-3}(2\pi c/a)$ and a strength of $\Delta\varepsilon/\varepsilon=1.63\times10^{-2}$. (c) Group delay spectra, with $\Delta\varepsilon/\varepsilon$ fixed at 1.63×10^{-2}. The blue, red, and green lines correspond to $\Omega=9.8\times10^{-3}$, 11.3×10^{-3}, and $12.8\times10^{-3}(2\pi c/a)$, respectively. (d) Group delay spectra, with Ω fixed at $9.8\times10^{-3}(2\pi c/a)$. The blue, red, and green lines correspond to $\Delta\varepsilon/\varepsilon=1.63\times10^{-2}$, 3.27×10^{-2}, and 6.53×10^{-2}. (e) Resonant frequency as a function of the modulation frequency. The blue and red circles corresponds to modulation strength of $\Delta\varepsilon/\varepsilon=1.63\times10^{-2}$ and 3.27×10^{-2}, respectively. Circles are simulation results as determined the peak location of group delay spectra, and the line is from analytical calculation. (f) Quality factor as a function of modulation strength. Circles are simulation results as determined from the peak width in (d), the line is from analytic calculation.

$\times10^{-3}(2\pi c/a)$, and a wavevector $q=0.196(2\pi/a)$), the transmission spectrum shows little change [Fig. 4(b)]. However, the group delay now exhibits a resonant peak with a quality factor $Q_e=1.09\times10^4$ [Fig. 4(c) blue line]. The structure indeed becomes a high-Q all-pass filter.

The properties of this resonance are controlled by the modulation. The resonant frequency changes linearly with respect to the modulation frequency, as predicted [Fig. 4(e)]. (When varying the modulation frequency, we also change the modulation wavevector at the same time to satisfy the phase-matching condition.) The resonance frequency is largely independent of the modulation strength [Fig. 4(e)]. The width of the resonance, and the peak delay, can be adjusted by changing the modulation strength [Fig. 4(d)]. As a comparison between theory [Eq. (9)] and simulations, Fig. 4(f) plots the quality factor as a function of the modulation strength at the fixed modulation frequency $\Omega=9.8\times10^{-3}(2\pi c/a)$. The simulation agrees excellently with the theory. The theory curve is generated with only one fitting parameter: the modal overlap factor $\kappa=0.99a^{-1}$, which agrees well to a direct and separate calculation of the well waveguide by itself that yields $\kappa=1.16a^{-1}$. The difference can be attributed to the finite-size effect of the well-barrier interfaces.

We now comment on some of the challenges in the practical implementations. For the simulated structure above, according to Eq. (9), a modulation strength of $\Delta\varepsilon/\varepsilon=5\times10^{-3}$, which is achievable using carrier injection in semiconductors,[13] results in an external quality factor of $Q_e=1.1\times10^5$. In comparison, the radiation quality factors of photonic crystal heterostructure cavities exceeded 10^6 in experiments.[14]

Regarding the required modulation frequencies, in the simulation, $\Omega=9.8\times10^{-3}(2\pi c/a)$ represents a modulation frequency of 8.1 THz, when the resonance frequency $\omega_0=0.235(2\pi c/a)$ corresponds to the wavelength of 1.55 μm. This is in principle achievable, since many index modulation scheme has intrinsic response time below 0.1 ps.[15] For modulation frequency of 10–100 GHz,[16,17] the proposed device provides a band-rejection resonant filter,[18] with the same independent control of resonant frequency and linewidth.

As final remarks, in our scheme, the tuning range for the resonant frequency is ultimately limited by the intrinsic response time of the material. Thus the resonant frequency of the structure have a much wider tuning range, and can be reconfigured with a much higher speed, compared with conventional mechanisms. Moreover, the modulation frequency can typically be specified to a much higher accuracy,[19] resulting in far more accurate control of the resonant frequency. Lastly, the localized state here is "dark" since it does not couple to the waveguide in the absence of modulation. Our scheme, which provides a dynamic access to such a dark state, is directly applicable for stopping and storage of light pulses, since the existence of a single dark state is sufficient.[20]

The work was supported by NSF (Grant No. ECS-0622212), and the NSF TeraGrid program that provides the computing facility.

[1]K. J. Vahala, Nature (London) **424**, 839 (2003).
[2]S. Fan, P. R. Villeneuve, J. D. Joannopoulos, and H. A. Haus, Phys. Rev. Lett. **80**, 960 (1998).
[3]D. Englund, A. Faraon, B. Zhang, Y. Yamamoto, and J. Vuckovic, Opt. Express **15**, 5550 (2007).
[4]M. F. Yanik, W. Suh, Z. Wang, and S. Fan, Phys. Rev. Lett. **93**, 233903 (2004).
[5]U. Fano, Phys. Rev. **124**, 1866 (1961).
[6]P. W. Anderson, Phys. Rev. **124**, 41 (1961).
[7]J. N. Winn, S. Fan, J. D. Joannopoulos, and E. P. Ippen, Phys. Rev. B **59**, 1551 (1999).
[8]P. Dong, S. F. Preble, J. T. Robinson, S. Manipatruni, and M. Lipson, Phys. Rev. Lett. **100**, 033904 (2008).
[9]D. F. Walls and G. J. Milburn, *Quantum Optics* (Springer, Berlin, 1994), Chap. 7, p. 123.
[10]B. Song, S. Noda, T. Asano, and Y. Akahane, Nature Mater. **4**, 207 (2005).
[11]Z. Yu and S. Fan, Nat. Photonics **3**, 91 (2009).
[12]A. Taflove and S. C. Hagness, *Computational Electrodynamics: The Finite-Difference Time-Domain Method*, 2nd ed. (Artech House, Boston, 2000).
[13]B. R. Bennett, R. A. Soref, and J. A. D. Alamo, IEEE J. Quantum Electron. **26**, 113 (1990).
[14]E. Kuramochi, M. Notomi, S. Mitsugi, A. Shinya, T. Tanable, and T. Watanabe, Appl. Phys. Lett. **88**, 041112 (2006).
[15]S. Schmitt-Rink, D. S. Chemla, W. H. Knox, and D. A. B. Miller, Opt. Lett. **15**, 60 (1990).
[16]L. Gu, W. Jiang, X. Cheng, and R. T. Chen, IEEE J. Sel. Top. Quantum Electron. **14**, 1132 (2008).
[17]Q. Xu, S. Manipatruni, B. Schmidt, J. Shakya, and M. Lipson, Opt. Express **15**, 430 (2007).
[18]Z. Yu and S. Fan (unpublished).
[19]T. W. Hänsch, Rev. Mod. Phys. **78**, 1297 (2006).
[20]C. Otey, M. L. Povinelli, and S. Fan, J. Lightwave Technol. **26**, 3784 (2008).